Precision Agriculture
https://doi.org/10.1007/s11119-022-09923-1

# A coupled atomization-spray drift model as online support tool for boom spray applications

**Carlos A. Renaudo**[1,2] · **Diego E. Bertin**[1,2] · **Verónica Bucalá**[1,2]

Accepted: 9 May 2022


## Abstract

The effectiveness of agrochemical products strongly depends on the capability of the atomized droplets to reach the target site in the desired amount. Spray drift is the movement of droplets downwind of the target area, and its minimization is a growing concern to ensure operator health, protect the environment, achieve efficient crop protection and transform the spraying of phytosanitary products into a sustainable activity. In this contribution, a coupled atomization-spray drift model suitable for different types of nozzles is developed and validated against experimental data. Particularly, the article focuses on providing a simple simulation tool, based on a minimum number of input data that are easily accessable to predict the ground deposition spray drift of a nozzle. It was found that the atomized droplets size distribution can be accurately predicted just as a function of the median volumetric diameter, which was successfully estimated as a function of spray pressure, nozzle nominal flowrate and spray angle (commonly known data). Besides, the proposed model, based on bivariate probability density functions, is able to accurately represent different physical phenomena using a low number of calculations. Its implementation is possible using low-resource computing systems as required for sprayer on-board software tools.

**Keywords** Spray drift · Atomization · Sprayer performance · Mathematical model

## List of symbols

| | |
|---|---|
| $a_{ul}$ | Parameter defined in Eq. 10 (–) |
| $A_n$ | Nozzle orifice area ($m^2$) |
| $C$ | Displacement of deposited droplets respect to $x_0$ (m) |
| $C_{PH}$ | Nozzle constant (m) |
| $C_d$ | Discharge coefficient (–) |
| $d$ | Droplet diameter (m) |
| $d_0$ | Atomized droplet diameter (m) |
| $d_{crit}$ | Critical droplet diameter (m) |
| $d_{dep}$ | Deposited droplet diameter (m) |

✉ Carlos A. Renaudo
carenaudo@plapiqui.edu.ar

[1] Departamento de Ingeniería Química, Universidad Nacional del Sur (UNS), Bahía Blanca, Argentina

[2] Planta Piloto de Ingeniería Química – PLAPIQUI (UNS-CONICET), Bahía Blanca, Argentina

Published online: 14 July 2022

| | |
|---|---|
| $d_{max}$ | Maximum diameter of atomized droplets (m) |
| $d_{min}$ | Minimum initial diameter of a droplet that reaches the soil surface (m) |
| $D_{V10}$ | Diameter where ten percent of the atomized droplets volume distribution has a smaller particle size (m) |
| $D_{V50}$ | Diameter where fifty percent of the atomized droplets volume distribution has a smaller particle size (m) |
| $D_{V90}$ | Diameter where ninety percent of the atomized droplets volume distribution has a smaller particle size (m) |
| $f_{x_0}$ | Volume distribution pattern of atomized droplets (1/m) |
| $f_{d,x_{dep}}$ | Density function of droplets with respect to the initial diameter and deposition distance (1/m) |
| $f_d$ | Density function of the atomized spray (1/m) |
| $f_{dep}$ | Density function of droplets with respect to the deposition distance (1/m) |
| $f_{d\alpha}$ | Bi-variate probability distribution (1/m rad) |
| $f_\alpha$ | Droplet trajectory angle distribution function (1/rad) |
| $F_d$ | Cumulative function of the atomized spray (–) |
| $F$ | Desired applied dose ($m^3/m^2$) |
| $g$ | Gravity acceleration constant ($m/s^2$) |
| $H$ | Nozzle height (m) |
| $k$ | Constant defined in Eq. 23 ($s/m^2$) |
| $Oh$ | Ohnesorge number (–) |
| $P$ | Atomization pressure (Pa) |
| $P_{ref}$ | Atomization pressure for which the nominal flowrate is specified (270 kPa for ISO 10625:2018 compliant nozzles) (Pa) |
| $Q$ | Nozzle volumetric flowrate ($m^3/s$) |
| $RH$ | Relative humidity (%) |
| $t$ | Time (s) |
| $t_{dep}$ | Deposition time of droplets (s) |
| $t_{resp}$ | Response time of a droplet (s) |
| $T$ | Wet bulb temperature (K) |
| $T_{bh}$ | Dry bulb temperature (K) |
| $\overline{U}$ | Representative wind speed of the total atomized droplets population (m/s) |
| $U$ | Wind speed (m/s) |
| $U_0$ | Wind speed at the nozzle height $H$ (m/s) |
| $v_A$ | Sprayer forward speed (m/s) |
| $v_T$ | Terminal velocity (m/s) |
| $w$ | Nominal spray width of a nozzle |
| $x$ | Spatial downwind coordinate (m) |
| $x_0$ | Spatial position of the volume distribution pattern (m) |
| $Y$ | Spray drift (–) |
| $z$ | Vertical co-ordinate (m) |

**Greek letters**

| | |
|---|---|
| $\alpha$ | Initial path angle of a drop (rad) |
| $\gamma$ | Wind speed constant (–) |
| $\delta$ | Nominal density function of droplets with respect to the deposition distance (1/m) |
| $\Delta T$ | Difference between dry and wet bulb temperatures (K) |
| $\epsilon$ | Roughness of the terrain (m) |

$\mu_g$ Air viscosity (Pa s)
$\theta$ Spray angle (rad)
$\rho_d$ Droplet density (kg/m$^3$)
$\rho_g$ Air density (kg/m$^3$)
$\sigma$ Surface tension (N/m)
$\sigma_{H_2O}$ Water surface tension (N/m)
$\sigma_s$ Standard deviation of $f_{x_0}$ (m)
$\sigma_{ul}$ Parameter defined in Eq. 9 (–)
$\Psi$ Nozzle parameter $\left(\mu m\left(\frac{m^3}{s}\right)^{-\frac{1}{3}}(Pa)^{\frac{1}{3}}(°)^{\frac{2}{3}}\right)$

## Introduction

Modern agriculture needs strategies to meet food security by increasing field crops productivity and quality (Pretty, 2008; Pretty & Bharucha, 2014). To this end, agrochemicals such as herbicides, insecticides, fungicides and fertilizers are commonly used (Onorato & Tesouro, 2006). These products are often applied as droplets, generated by ground or aerial spray application systems (van den Berg et al., 1999). During application, only a fraction of the droplets is deposited in the target area. This agrochemical loss can range from a few percentage points to 30% or even more than 50% (van den Berg et al., 1999). The causes of these losses include spray drift (movement of droplets downwind of the target area), vapor drift (volatilization of the active component), runoff (no absorption of the active component deposited in the target area, which is lost across the soil surface) and leaching (movement of agrochemical in water through the soil) (Srivastava et al., 2009). Particularly, spray drift is defined as the physical movement of the droplets through air from the target site to any off-target area caused by the wind or air disturbances (BCPC, 1986; EPA, 2001; International Organization for Standardization, 2008).

The losses caused by spray drift depend on several variables such as sprayer technology, properties of the sprayed solution, weather and operating conditions and applicator expertise (Matthews et al., 2014). Nowadays, multiple sensors (such as weather stations, GNSS, cameras and pressure transducers) are available at relatively low cost and can be used as a source of real-time data of interest for applicators (Song et al., 2015). However, even though they would have access to many variable values, some applicators may not have experience for proper decision making (Bish & Bradley, 2017). Therefore, there is a large opportunity to develop software for real-time applicators assistance using sensed data to develop smart farming technologies (Villa-Henriksen et al., 2020).

In this context, a validated mathematical model capable of predicting the deposited volume of agrochemicals based on process variables (which can be either set or sensed) becomes a fundamental tool to define appropriate application conditions. The model integrated to a sprayer software can provide to the applicator, in real time, information to monitor and/or control agrochemical losses. Calculation of the key sprayer performance indicators (e.g., impacts/mm$^2$, evaporation, spray drift) would allow the system to show and present alerts *ex ante* about the occurrence of severe spray drift (Fig. 1). In advanced units, the sprayer software can be integrated with sensors and actuators for automatic control of the process, which can be a powerful tool for non-highly trained applicators.

To model the spray drift process, mathematical representations of the atomization step and spray drift itself are required. The models can be classified into empirical and phenomenological ones. The latter [Lagrangian, dispersion and computational fluid dynamic

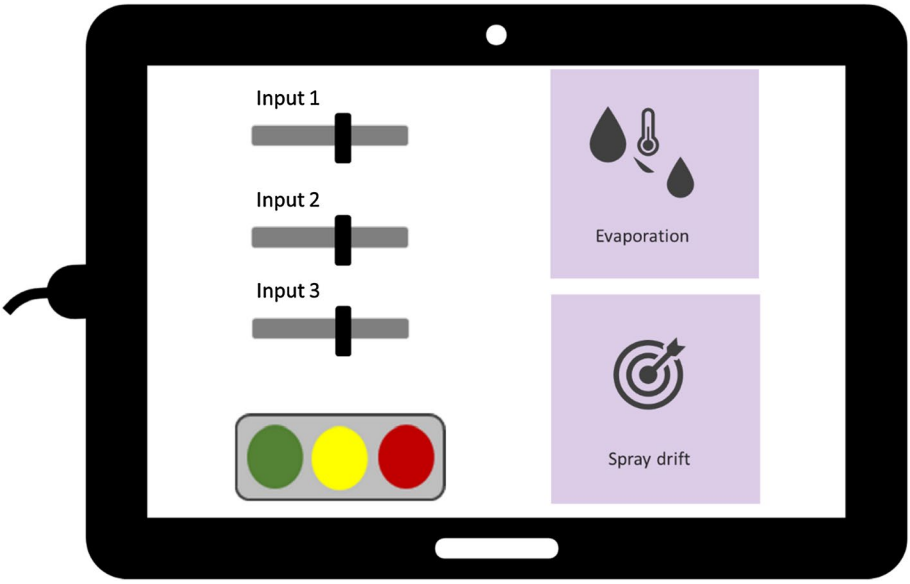


**Fig. 1** Software interface. Data input and examples of key performance indicators (KPI)

(CFD) models] emerge as the more suitable tools to achieve a greater understanding of the spray drift phenomenon, provide a systematic tool for regulatory use and optimize the atomization operation (Teske et al., 2011). Lagrangian models track the trajectory and size of individual droplets, while dispersion models give, as a direct result, the spatial cloud droplets concentration (Stainier et al., 2006; Tan, 2014). In CFD models, the air velocity profile is obtained by solving the Navier–Stokes equations and then these velocities are used to solve the droplets force and mass balances. Within the Lagrangian, dispersion and CFD models, the first two demand the lowest computational cost. All the phenomenological models require the atomized droplet size distribution (DSD) as input data. However, low computational cost models coupling the mathematical representation of the atomization- spray drift processes are scarce.

In this contribution, a coupled atomization-spray drift model suitable for different types of nozzles is developed and validated against experimental data. This article provides a simple tool, that requires a minimum number of easily accessible input data and can be implemented in low-resource computing systems, to predict the ground deposition spray drift of a nozzle. This information is very valuable for applicators and automatic control systems to avoid unsafe operations.

## Materials and methods

A combined atomization-spray drift mathematical model is proposed to be used as a component of sprayer software (schematically illustrated in Fig. 2). The software prototype, that requires a reduced number of input data, is divided into five modules and the input variables are indicated in light grey boxes. The first module, the DSD Predictor, allows calculation of the atomized DSD based on: the operating pressure and the selected nozzle model (i.e., nozzle

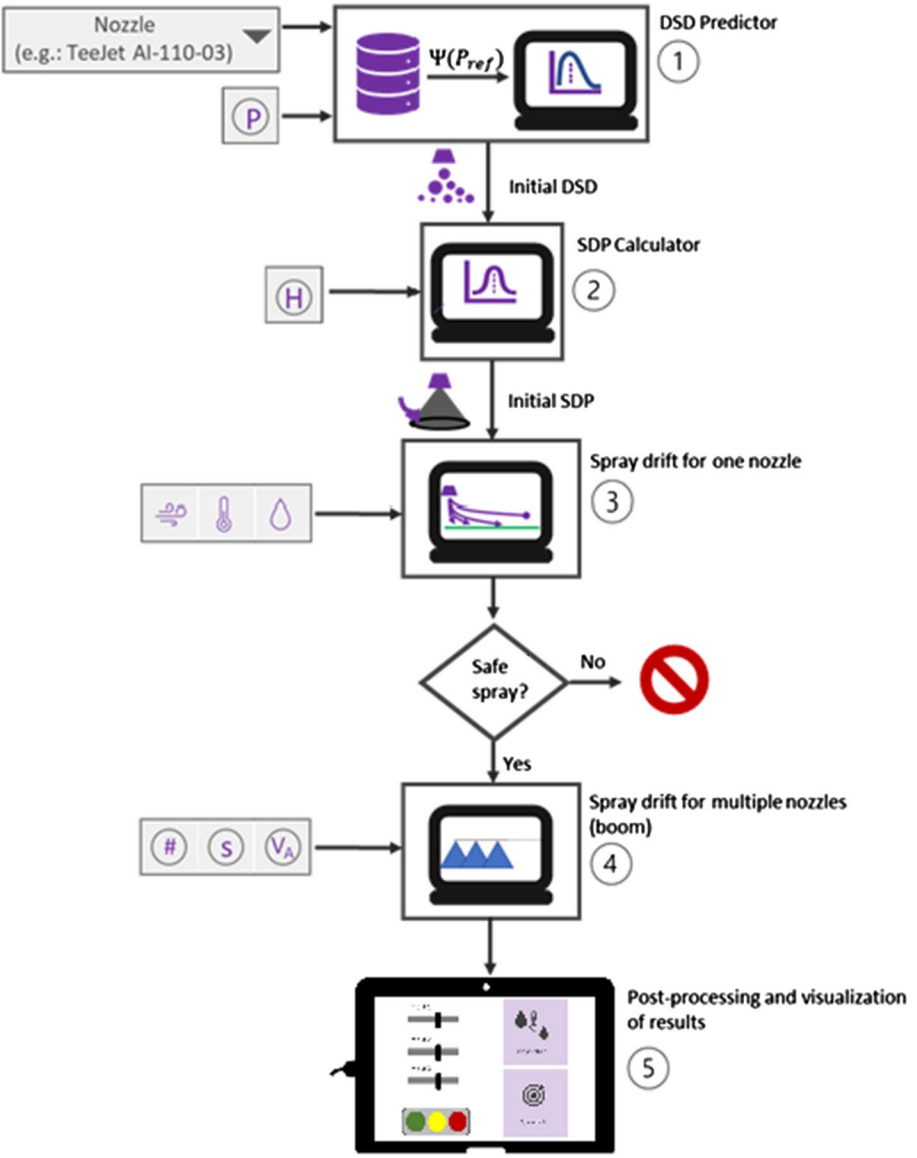


**Fig. 2** Calculation steps to provide spray KSPIs

type, angle and size). In the second module, the spray distribution pattern (SDP) is predicted based on the calculated DSD and the nozzle height. The information calculated in modules 1 and 2 in combination with the weather conditions (temperature, relative humidity and wind speed and direction) are used in module 3 to predict the droplet deposition generated by a single nozzle. The results of module 3 allows the calculation of the desired key sprayer performance indicators (KSPIs) for a given nozzle. Since ground spraying is usually done using boom sprayers with multiple nozzles, module 3 has to be applied to all the nozzles located

at different positions (Renaudo, 2020). If the spray drift is greater than an allowed value, an alert signal can be sent to the applicator to perform a corrective action (or under closed control loop, eventually an automatic action could be performed). If the spray drift given by one nozzle is unacceptable, the application has to be aborted. In this way, the software executes an early exit for a prompt response. However, if the calculated spray drift of one nozzle is low, the contribution of the complete set of nozzles has to be calculated to estimate the real ground deposition spray drift. The last action, that is more computer time consuming, is not required to be done for all the operating conditions windows.

## Mathematical model

### Atomized droplet size distribution—DSD predictor

The spray drift models run with multiple inputs, including the emission droplet size spectrum, that is usually given by experimental assays. Since the DSD is a function of many properties and variables, many experiments would be required to develop sprayer software useful for different applications. The fast adoption of spray drift models on online support tools depends on the use of a limited number of easily accessible input data. In this way, a simplified method to calculate the DSD is hereafter proposed.

The median volume diameter is usually used to characterize the atomized spray (da Cunha et al., 2019). In fact, the ASABE S572.1 standard classifies the atomized spray as a function of this parameter (ASABE, 2009). While the information regarding droplet size provided by ASABE S572.1 standard may be enough for nozzle selection, this level of information is insufficient for spray drift modelling purposes.

Numerous correlations have been reported to estimate mean droplet sizes (e.g., the median diameter) in terms of dimensionless numbers such as Reynolds (*Re*), Weber (*We*) and Ohnesorge (*Oh*), which include operating variables (e.g., atomization pressure), fluid properties and nozzle design (Ashgriz, 2011; Lefebvre & McDonell, 2017). In particular, Post and Hewitt (2018) developed an expression that allows the calculation of the mean volume diameter ($D_{V50}$) produced by agricultural nozzles as follows:

$$D_{V50} = C_{PH}\left(\frac{Q(P_{ref})}{6.3110^{-6}\mathrm{m^3s^{-1}}}\right)^{\frac{1}{3}}\left(\frac{P}{10^5 Pa}\right)^{-\frac{1}{3}}\left(\frac{\theta}{110}\right)^{-\frac{2}{3}}\left(\frac{\sigma}{\sigma_{H_2O}}\right)^{\frac{1}{3}} C_d{}^{-\frac{2}{3}} f(Oh) \quad (1)$$

To predict $D_{V50}$ of a spray generated by a given nozzle, it is necessary to know the nozzle constant and discharge coefficient,$C_{PH}$ and $C_d$, respectively. These parameters can be estimated using experimental data or, if available, information provided by nozzle manufacturers. Equation 1 also requires knowledge of the atomized flowrate $Q$ at a given reference pressure $P_{ref}$ (i.e., nominal flowrate). Post and Hewitt (2018) validated Eq. 1 for TeeJet air induction and flat-fan nozzles using measured $D_{V50}$ values. They found good agreement between the experimental and calculated data.

For a selected nozzle, Eq. 1 can be rewritten as:

$$\frac{D_{V50}}{D_{V50}^{+}} = \frac{C_{PH}\left[\frac{Q(P_{ref})}{6.3110^{-6}m^3s^{-1}}\right]^{\frac{1}{3}}\left(\frac{P}{10^5Pa}\right)^{-\frac{1}{3}}\left(\frac{\theta}{110}\right)^{-\frac{2}{3}}\left(\frac{\sigma}{\sigma_{H_2O}}\right)^{\frac{1}{3}}C_d{}^{-\frac{2}{3}}f(Oh)}{C_{PH}^{+}\left[\frac{Q^{+}(P_{ref})}{6.3110^{-6}\mathrm{m}^3\mathrm{s}^{-1}}\right]^{\frac{1}{3}}\left(\frac{P^{+}}{10^5Pa}\right)^{-\frac{1}{3}}\left(\frac{\theta^{+}}{110}\right)^{-\frac{2}{3}}\left(\frac{\sigma^{+}}{\sigma_{H_2O}}\right)^{\frac{1}{3}}\left(C_d^{+}\right)^{-\frac{2}{3}}f(Oh^{+})} \tag{2}$$

where the superscript + applies to the same nozzle model at different operating conditions and spraying eventually a different fluid.

For a given nozzle model and if the same solution is atomized, $C_{PH}, C_d, \sigma$ and $f(Oh)$ can be assumed constant (Post & Hewitt, 2018; Renaudo, 2020). Based on these considerations, Eq. 2 becomes:

$$D_{V50} = \Psi\left[Q(P_{ref})\right]^{\frac{1}{3}}P^{-\frac{1}{3}}\theta^{-\frac{2}{3}} \tag{3}$$

where $\Psi$ is given by the following expression:

$$\Psi = D_{V50}^{+}\left[Q^{+}(P_{ref})\right]^{-\frac{1}{3}}\left(P^{+}\right)^{\frac{1}{3}}\left(\theta^{+}\right)^{\frac{2}{3}} \tag{4}$$

Equation 3 indicates that the volumetric median diameter ($D_{V50}$) of a given nozzle model could be predicted as a function of $Q\left(P_{ref}\right), P$ and $\theta$ if $\Psi$ is known. To obtain the $\Psi$ value, experimental information about just one volumetric median diameter obtained from a measured DSD emitted from the same nozzle model operating at known conditions ($Q^{+}(P_{ref}), P^{+}$ and $\theta^{+}$) is necessary. In other words, a $\Psi$ value is required for each nozzle model. However, this value can be estimated just with a single experiment, reducing the needed data dramatically. Once $\Psi$ is known, the $D_{V50}$ of a given model nozzle can be estimated without requiring further experimentation. As reported by Sijs et al. (2021), there may be differences in the measured DSDs by different methods, then $\Psi$ is measurement technique dependent. Therefore, Eq. 3 predicts a $D_{V50}$ of a DSD equivalent to the one that would have been measured using the same technique than the one employed to determine the $\Psi$ value. The accuracy of this approach is discussed below.

To validate Eq. 3, experimental data of $D_{V50}, Q(P_{ref}), P$ and $\theta$ reported in the literature were used. As mentioned, the $\Psi$ parameter is expected to be influenced by the DSD measurement technique used. Because of this, for each method and nozzle model, a different $\Psi$ value was calculated. To this end, data from 32 nozzle models of 5 brands were used (Czaczyk, 2012; Gil et al., 2014; Guler et al., 2012; Nuyttens et al., 2007, 2009; van de Zande et al., 2002, 2008; Wang et al., 2015). In all the cases, the atomized solution was water. The details of the characteristics of the nozzle and DSD measurement technique for each dataset are shown in Table 1.

Of each dataset in Table 1, one single experiment was used to obtain the $\Psi$ parameter (see Eq. 4), while the remaining data (102 experimental points) were employed for $D_{V50}$ prediction by using Eq. 3 (i.e., for model validation). Within the datasets, there are different nozzles, nominal flowrates, spray angles and operating pressures.

Figure 3 compares the experimental and calculated $D_{V50}$ values; different markers are used to distinguish the different DSD measurement techniques. Independently of those techniques, volumetric median diameters are well predicted over a range between 150 and 600 µm. Therefore, for $D_{V50}$ between 150 and 600 µm, Eq. 3 extends the validity of the correlation originally presented by Post and Hewitt (2018) to other nozzle brands, types and spray patterns.

**Table 1** Nozzle datasets

| References | Equipment | Technique | Nozzle brand | Nozzle models |
|---|---|---|---|---|
| Czaczyk (2012) | Sympatec HELOS Vario (Sympatec GmbH, Clausthal-Zellerfeld, Germany) | Laser Diffraction (LD) | Albuz | AXI |
| | | | MMAT | AZ; RS |
| Gil et al. (2014) | Malvern Spraytec (Malvern Instruments Ltd., Worcestershire, UK) | Laser diffraction (LD) | TeeJet | AIXR |
| | | | | XR |
| Guler et al. (2012) | VisiSizer and PIV (Oxford Lasers Inc., Didcot, UK) | Particle Image Velocimetry (PIV) | TeeJet | AI; AM; D5-DC25; TJ; TP; TT; TTD; XR |
| Nuyttens et al. (2007) | Aerometrics PDPA (TSI, Inc., Minneapolis, USA) | Phase Doppler Particle Analyzer (PDPA) | Albuz | ATR80; API; AXI; ADI; AVI |
| | | | Hardi | ISO F; ISO LD; ISO Injet |
| van de Zande et al. (2002) | Aerometrics PDPA (TSI, Inc., Minneapolis, USA) | Phase Doppler Particle Analyzer (PDPA) | Lechler | LU |
| | | | Teejet | XR |
| van de Zande et al. (2008) | Aerometrics PDPA (TSI, Inc., Minneapolis, USA) | Phase Doppler Particle Analyzer (PDPA) | Lechler | ID |
| | | | Teejet | AI; DG |
| Wang et al. (2015) | Custom PIV | Particle Image Velocimetry (PIV) | Lechler | IDK; ST; TR |

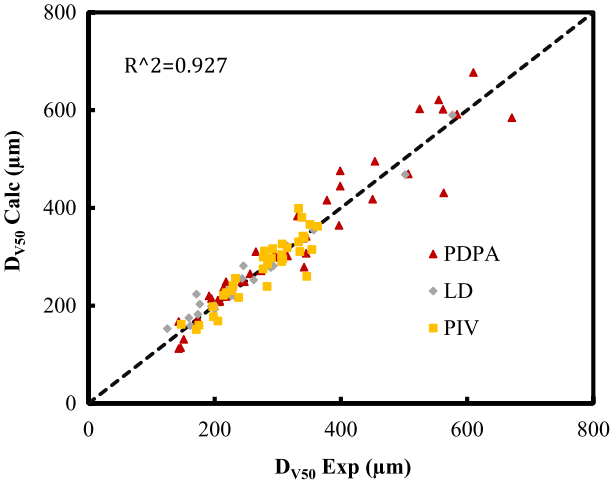


**Fig. 3** Experimental and calculated $D_{V50}$ values. The experimental data correspond to experiments using different nozzle designs (flat fan, hollow cone, twin, among others) and spray angles (80º, 110º, 120°, among others)

In the literature, data about $D_{V10}$ and $D_{V90}$ (i.e., diameters for which the droplets population is below 10 and 90% of the total volume, respectively) of sprays produced by agricultural nozzles are also available (Czaczyk, 2012; Gil et al., 2014; Guler et al., 2012; Nuyttens et al., 2007, 2009; van de Zande et al., 2002, 2008; Wang et al., 2015). Figure 4 shows the characteristic sizes $D_{V10}$ (Fig. 4a) and $D_{V90}$ (Fig. 4b) as a function of $D_{V50}$ for different experimental DSDs reported by the above-mentioned authors. The $D_{V10}$ and $D_{V90}$ diameters can be satisfactorily correlated as a function of $D_{V50}$ using linear regression models as presented in Eqs. 5 and 6, respectively.

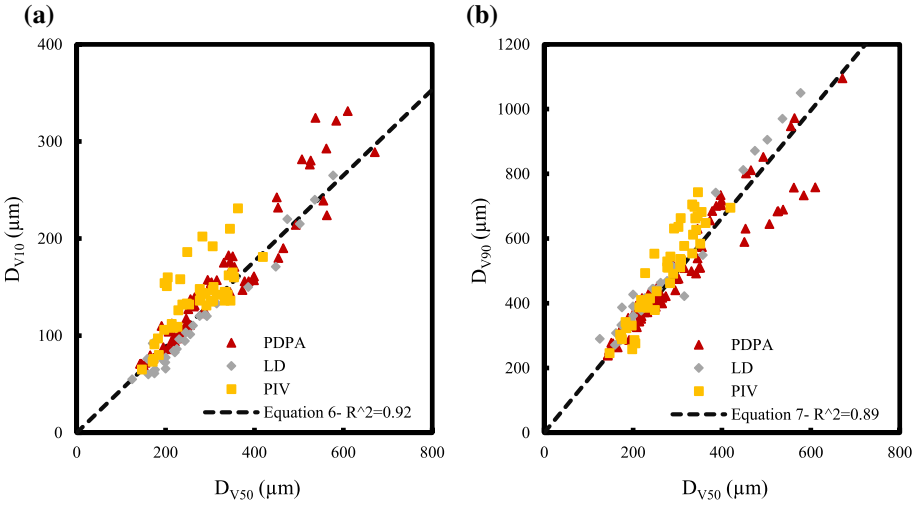


**Fig. 4** Experimental and calculated $\boldsymbol{D_{V10}}$ and $\boldsymbol{D_{V90}}$ as a function of $\boldsymbol{D_{V50}}$. The experimental data correspond to experiments using different nozzle designs (flat fan, hollow cone, twin, among others) and spray angles (80°, 110°, 120°, among others)

$$D_{V10} = 0.44 D_{V50} \tag{5}$$

$$D_{V90} = 1.66 D_{V50} \tag{6}$$

For agricultural nozzles, Hong et al. (2018) reported that DSDs can be well described by the upper-limit log normal (ULLN) function. The ULLN represents the volume density function to find droplets of a specific diameter ($d_0$) in the atomized DSD, and is given by:

$$f_d(d_0) = \begin{cases} \frac{1}{\sqrt{2\pi} ln\sigma_{ul}} \frac{d_{max}}{d_0(d_{max}-d_0)} e^{-\frac{1}{2}\left[\frac{ln(a_{ul}d_0)-ln(d_{max}-d_0)}{ln\sigma_{ul}}\right]^2} & d < d_{max} \\ 0 & d \geq d_{max} \end{cases} \tag{7}$$

$$d_{max} = D_{V50}\left(\frac{D_{V50}\left(D_{V10}+D_{V90}\right) - 2D_{V10}D_{V90}}{\left(D_{V50}\right)^2 - D_{V10}D_{V90}}\right) \tag{8}$$

$$\sigma_{ul} = \left[\left(\frac{d_{max}-D_{V50}}{d_{max}-D_{V90}}\right)\frac{D_{V90}}{D_{V50}}\right]^{0.7794} \tag{9}$$

$$a_{ul} = \frac{d_{max}-D_{V50}}{D_{V50}} \tag{10}$$

As can be seen, the ULLN parameters (Eqs. 8 to 10) are functions of different characteristic diameters of the DSD. Considering the correlations given by Eqs. 5 and 6, the ULLN parameters become:

$$d_{max} = 2.36 D_{V50} \tag{11}$$

$$a_{ul} = 1.36 \tag{12}$$

$$\sigma_{ul} = 2.51 \tag{13}$$

Replacing Eqs. 11–13 in Eq. 7, the ULLN function can be expressed as:

$$f_d(d_0) = \begin{cases} \frac{1}{\sqrt{2\pi} ln2.51} \frac{2.36D_{V50}}{d_0(2.36D_{V50}-d_0)} e^{-\frac{1}{2}\left[\frac{ln(1.36d_0)-ln(2.36D_{V50}-d_0)}{ln2.51}\right]^2} & d < d_{max} \\ 0 & d \geq d_{max} \end{cases} \tag{14}$$

The corresponding cumulative function can be calculated as follows:

$$F_d(d_0) = \begin{cases} 0 & d_0 < 0 \\ \frac{1}{2}\left(1 - erf\left(\frac{ln(2.36D_{V50}-d_0)-ln(1.36d_0)}{\sqrt{2}ln(2,51)}\right)\right) & 0 \leq d_0 < d_{max} \\ 1 & d_0 \geq d_{max} \end{cases} \tag{15}$$

Summarizing, the approach developed to predict the $D_{V50}$ of a DSD produced by a given nozzle model and operating conditions, also allows the prediction of the complete

atomized DSD in a simple manner. This development simplifies the input data for spray drift simulation and therefore contributes towards the improvement of sprayer software for precision agriculture.

## Spray distribution pattern—SDP predictor

The spray distribution pattern is widely used for spray performance assessment (Kluza et al., 2019) and its calculation is a key step to approximate the droplet initial trajectories distribution. As is shown in Fig. 5a, a patternator can be used to experimentally collect the sprayed droplets from a nozzle (located at a height $H$) in the $x$-direction (Butts et al., 2019). To build the distribution, normalized collectors and measurement methods are commonly used to quantify the deposited volume fraction at each distance (Matthews et al., 2014). With this information, a probability density function ($f_{x_0}(x_0)$) can be obtained as shown in Fig. 5b.

$f_{x_0}(x_0)$ is usually represented by means of a Gaussian distribution function (Mawer & Miller, 1989):

$$f_{x_0}(x_0) = \frac{1}{\sqrt{2\pi}\sigma_s}\exp\left[-\frac{1}{2}\left(\frac{x_0}{\sigma_s}\right)^2\right] \tag{16}$$

Due to the fact that $f_{x_0}(x_0)$ has to be negligible for $x_0$ distances outside of the limits of the spray, $\sigma_s$ is arbitrarily set so that Eq. 17 is satisfied (Leunda et al., 1990; Mawer & Miller, 1989):

$$f_{x_0}\left(\frac{w}{2}\right) = f_{x_0}\left(-\frac{w}{2}\right) = 1e^{-6} \tag{17}$$

If the wind speed is negligible, according to Fig. 5a, the distance ($x_0$) at which each droplet with initial angle ($\alpha$) is deposited can be calculated as:

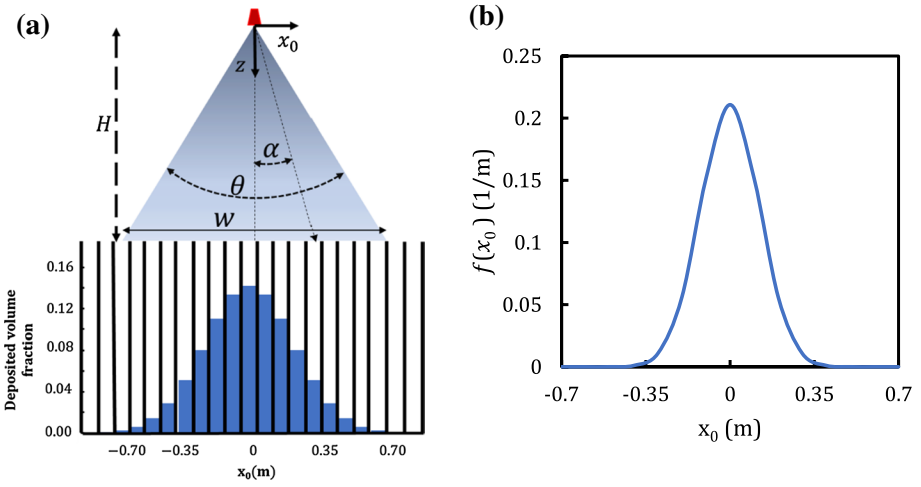


**Fig. 5** **a** Paternattor schematic view, **b** deposited volume density function

$$x_0 = Htan\alpha \tag{18}$$

By using Eqs. 16 and 18, the droplet trajectory angle distribution function $f_\alpha(\alpha)$ can be expressed as a function of the volume distribution pattern as follows:

$$f_\alpha(\alpha) = \frac{dx_0}{d\alpha} f_{x_0}(x_0) = \frac{H^2 + {x_0}^2}{H} f_{x_0}(x_0) \tag{19}$$

The probability of a droplet having a determined initial size and angle can be described by using a bi-variate probability distribution:

$$f_{d\alpha}(d_0, \alpha) = f_d(d_0) f_\alpha(\alpha | d_0) \tag{20}$$

where $f_\alpha(\alpha|d_0)$ is the conditional distribution of $\alpha$ given $d_0$. If the initial direction is assumed to be independent of the initial droplet diameter, $f_\alpha(\alpha|d_0)$ is equal to $f_\alpha(\alpha)$.

Replacing Eqs. 14 and 19 in Eq. 20, the two-dimensional function that represents the distribution of the atomized drops with respect to the diameter and the initial trajectory becomes:

$$f_{d\alpha}(d_0, \alpha) = \begin{cases} \frac{H(1+(\tan\alpha)^2)}{2\pi\sigma_s ln\sigma_{ul}} \frac{d_{max}}{d_0(d_{max}-d_0)} e^{-\frac{1}{2}\left\{\left[\frac{ln(a_{ul}d_0)-ln(d_{max}-d_0)}{ln\sigma_{ul}}\right]^2 + \left(\frac{H\tan\alpha}{\sigma_s}\right)^2\right\}} & d_0 < d_{max} \\ 0 & d_0 \geq d_{max} \end{cases} \tag{21}$$

## Spray drift model

**Droplet deposition model** The deposition model is based on the following hypothesis:

1. Atomization and deposition of droplets occur in steady state.
2. Droplets are spherical and have constant viscosity and density.
3. The average droplet velocity in the downwind direction is a function of the wind velocity profile and the atomized droplet sizes.
4. In the vertical direction ($z$), the velocity of a droplet of a given size is equal to the corresponding terminal velocity ($v_T$) (Lebeau et al, 2011; Løfstrøm et al., 2013).
5. In the horizontal direction ($x$), the velocity of the droplets is equal to the wind one (Løfstrøm et al., 2013).
6. Droplets are deposited as soon as they reach the soil surface.
7. The active ingredient of droplets is present in low concentration and has lower volatility than water. Hence, evaporation of pure water is considered (Teske et al., 2016).
8. The field is flat, with low crop density and low surface roughness. Droplets are affected by wind turbulence even close to the ground.

The droplet deposition model was developed considering the above assumptions and equations and parameters previously reported (see Table 2). Equations 22–24 are related to the evaporation phenomena while Eqs. 25–27 provide tools to calculate droplet deposition distances.

Some other equations were developed for the spray drift model presented in this article and are detailed in Table 3. The methodology to obtain those equations can be found elsewhere (Renaudo, 2020). Equation 28 relates the height at which there is a droplet

**Table 2** Physical phenomena mathematical description and parameters

| Description | Equation | References |
|---|---|---|
| Droplet size change due to evaporation | $d = \begin{cases} d_0\left(1 - \frac{t}{kd_0{}^2}\right) & t < kd_0{}^2 \\ 0 & t \geq kd_0{}^2 \end{cases}$ (22) | Lebeau et al. (2011) and Onorato and Tesouro (2006) |
| Evaporation rate constant | $k = \frac{1.2510^9 \frac{s^\circ C}{m^2}}{(T - T_{bh})}$ (23) | Lebeau et al. (2011) |
| Wet bulb temperature | $T_{bh} = Ttan^{-1}\left(0.15\sqrt{RH + 8.31}\right) + tan^{-1}(T + RH)$ $-tan^{-1}(RH - 1.68) + 3.91.10^{-3}RH^{\frac{3}{2}}tan^{-1}(0.0231RH) - 4.69$ (24) | Stull (2011) |
| Wind velocity profile | $U = U_0 \frac{\ln\left(\frac{(H-z)+\epsilon}{\epsilon}\right)}{\ln\left(\frac{H+\epsilon}{\epsilon}\right)}$ (25) | Tan (2014) |
| Terminal velocity (Stoke regime) | $\frac{dz}{dt} = v_T = \frac{(\rho_d - \rho_g)gd^2}{18\mu_g}$ (26) | Zannetti (2013) |
| Response time of a droplet to fluid motion (Stoke regime) | $t_{resp} = \frac{\rho_d d_0{}^2}{18\mu_g}$ (27) | Hughes (2013) and Bodnár et al. (2017) |

**Table 3** Auxiliary equations (Renaudo, 2020)

| Description | Equation |
|---|---|
| Droplet vertical position | $z = -kd_0 \frac{(\rho_d - \rho_g)g}{54\mu_g} \left(d^3 - {d_0}^3\right)$ (28) |
| Droplet deposition time | $t_{dep} = k{d_0}^2 \left[1 - \left(1 - \frac{54\mu_g H}{k{d_0}^4(\rho_d - \rho_g)g}\right)^{\frac{1}{3}}\right]$ (29) |
| Droplet deposition diameter | $d_{dep} = d_0 \left(1 - \frac{54\mu_g H}{k{d_0}^4(\rho_d - \rho_g)g}\right)^{\frac{1}{3}}$ (30) |
| Minimum initial droplet diameter that is deposited | $d_{min} = \left(\frac{54\mu_g H}{k(\rho_d - \rho_g)g}\right)^{\frac{1}{4}}$ (31) |
| Droplet critical diameter | $d_{crit} = \left[\frac{54\mu_g H}{k(\rho_d - \rho_g)g} \frac{1}{1 - \left(1 - \frac{\rho_d}{k18\mu_g}\right)^3}\right]^{1/4}$ (32) |
| Droplet deposition distance | $x_{dep} = x_0 + \overline{U} t_{dep}$ (33) |

of diameter $d$, whose initial diameter was equal to $d_0$. According to Eq. 29, droplets of different initial sizes $d_0$ will have different deposition times. In Eq. 30, if $d_{dep} \leq 0$ implies that the droplet with an initial diameter $d_0$ completely evaporates before reaching the objective surface (i.e., before traveling distance $H$). Therefore, for $d_{dep} = 0$, the minimum initial diameter of a droplet that reaches the soil surface can be calculated (Eq. 31). Droplets with response times (Eq. 27) higher than the deposition ones are less likely to be influenced by the wind. The diameter of a droplet of equal response and deposition times, called critical diameter ($d_{crit}$), is given by Eq. 32. As stated by hypothesis 3, the wind velocity is considered constant in this model. According to Eq. 33, the deposition distance ($x_{dep}$) have two contributions: the initial droplet trajectory ($x_0$) and the distance that the wind dragged the droplet ($\overline{U} t_{dep}$).

Replacing Eq. 28 (which relates the vertical position of a droplet with its initial and actual diameters $d_0$ and $d$, respectively) in Eq. 25, the following expression is obtained:

$$U = U_0 \frac{\ln\left\{1 + \frac{H}{\epsilon} + \frac{k\Delta\rho g {d_0}^4}{54\mu_g \epsilon}\left[\left(1 - \frac{t}{k{d_0}^2}\right)^3 - 1\right]\right\}}{\ln\left(\frac{H+\epsilon}{\epsilon}\right)} \tag{34}$$

If the diameter $d$ is replaced by Eq. 22, Eq. 34 becomes:

$$U = U_0 \frac{\ln\left\{1 + \frac{H}{\epsilon} + \frac{k\Delta\rho g {d_0}^4}{54\mu_g \epsilon}\left[\left(1 - \frac{t}{k{d_0}^2}\right)^3 - 1\right]\right\}}{\ln\left(\frac{H+\epsilon}{\epsilon}\right)} \tag{35}$$

Equation 35 allows to obtain the wind speed U for any droplet with initial diameter $d_0$ as a function of time. To obtain a mean wind speed value for all the droplets, the above equation must be averaged with respect to time and diameter (considering the DSD):

$$\overline{U} = \frac{\int_{d_{min}}^{d_{crit}} \int_{t_0}^{t_{dep}} U f_d(d_0) dt d d_0}{\int_{d_{min}}^{d_{crit}} \int_{0}^{t_{dep}} f_d(d_0) dt d d_0} \tag{36}$$

The integration limits of Eq. 36 were selected to consider only those droplet diameters that are deposited and affected by the wind (i.e., droplet sizes between $d_{min}$ and $d_{crit}$), and the time period in which the droplets are carried by the wind (between 0 and $t_{dep}$).

Considering Eqs. 35, 36, can be represented as:

$$\overline{U} = \gamma U_0 \tag{37}$$

where $\gamma$ varies between 0 and 1 and depends only on the dynamics of droplets movement:

$$\gamma = \ln\left(-\frac{H+\epsilon}{\epsilon}\right) \frac{\int_{d_{min}}^{d_{crit}} \int_{0}^{t_{dep}} \ln\left\{1 + \frac{H}{\epsilon} + \frac{k d_0 \Delta \rho g {d_0}^3}{54 \mu_g \epsilon}\left[\left(1 - \frac{t}{k d_0^2}\right)^3 - 1\right]\right\} f_d(d_0) dt d d_0}{\int_{d_{min}}^{d_{crit}} \int_{0}^{t_{dep}} f_d(d_0) dt d d_0} \tag{38}$$

Equation 38 was solved for different DSDs represented by Eq. 14 (with $D_{V50}$ varying between 50 and 1000 μm) and different atmospheric conditions (temperatures between 1 and 35 °C, RHs between 10 and 99%), boom heights between 0.35 and 0.7 m, and sprayed solution densities between 900 and 1100 kg/m$^3$. Evaluating the resulting $\gamma$ values, it was found that this parameter was mainly affected by $D_{V50}$ and it was successfully correlated (data not shown, $R^2 = 0.947$) as follows:

$$\gamma = 0.04 {D_{V50}}^{-0,28} \tag{39}$$

In Eq. 39, the units of $D_{V50}$ are meters in order to obtain a dimensionless $\gamma$ value.

By using Eq. 39 instead of Eq. 38, the need to solve a numerical integration for each simulation is avoided. Then, the required computational time is reduced.

## Deposited volume distribution function

Deriving Eq. 33 with respect to the initial droplet angle ($\alpha$), using the chain rule and Eq. 19, the following equation is obtained:

$$\frac{\partial x_{dep}}{\partial \alpha} = \frac{\partial x_{dep}}{\partial x_0} \frac{dx_0}{d\alpha} = H\left[1 + (\tan\alpha)^2\right] \tag{40}$$

where $\frac{\partial x_{dep}}{\partial x_0} = 1$ (see Eq. 33).

By means of a variable change in Eq. 21, which provides the volume distribution as a function of initial size and angle, it is possible to describe the deposited volume distribution:

$$f_{d,x_{dep}}(d_0, x_{dep}) = \frac{\partial \alpha}{\partial x_{dep}} f_{d\alpha}(d_0, \alpha) \tag{41}$$

Replacing Eqs. 21 and 40 in Eq. 41, the bi-variate density function that represents the distribution of the atomized drops with respect to the diameter and the deposited distance becomes:

$$f_{d,x_{dep}}\left(d_0, x_{dep}\right) = \begin{cases} \frac{1}{2\pi\sigma_s ln\sigma_{ul}} \frac{d_{max}}{d_0\left(d_{max}-d_0\right)} e^{-\frac{1}{2}\left\{\left[\frac{ln\left(a_{ul}d_0\right)-ln\left(d_{max}-d_0\right)}{ln\sigma_{ul}}\right]^2+\left(\frac{x_{dep}-C}{\sigma_s}\right)^2\right\}} & d_0 < d_{max} \\ 0 & d_0 \geq d_{max} \end{cases} \tag{42}$$

Equation 42 describes the probability in volume of active ingredient to find a deposited droplet of a given size ($d_0$) at a given downwind distance ($x_{dep}$). The marginal distribution on $x_{dep}$ of Eq. 42 is calculated as follows:

$$f_{dep}\left(x_{dep}\right) = \int_{d_{min}}^{d_{max}} f_{d,x_{dep}}\left(d_0, x_{dep}\right) dd_0 \tag{43}$$

## Spray drift

Considering hypothesis 1 (steady state) and the operating conditions (atomized flow rate, $Q$, and sprayer speed, $v_A$), the volume deposited per unit area at a given distance is calculated as follows:

$$\frac{V_{dep}}{A} = \frac{Q}{v_A} f_{dep}\left(x_{dep}\right) \tag{44}$$

Deposition spray drift is defined as the ratio between the volume deposited per unit area and the dosage:

$$Y\left(x_{dep}\right) = \frac{\frac{V_{dep}}{A}}{F} = \frac{\frac{Q}{v_A} f_{dep}\left(x_{dep}\right)}{F} \tag{45}$$

The nozzle flowrate ($Q$), as a continuous variable, can be calculated as Post et al. (2017):

$$Q = C_d A_n \sqrt{\frac{2P}{\rho_d}} \tag{46}$$

For nozzles that follow the ISO 10625:2018 standard, the flowrate $Q$ can be calculated using the $C_d A_n$ for different ISO color codes as shown in Table 4.

The model was solved using the Python 3.8 programming language. Regarding the solving process, first, for a given nozzle and operating pressure, the set of algebraic equations constituted by Eqs. 3, 11–13 and 17 is solved to estimate the atomized DSD. Once the climatic conditions are defined, the evaporation rate constant is then calculated (Eqs. 23 and 24). Thirdly, the droplet diameters $d_{min}$ and $d_{crit}$ (Eqs. 31 and 32) and the mean wind speed $\overline{U}$ (Eqs. 37 and 39) are estimated. To obtain the deposition function $f_{dep}$ at a given distance $x_{dep}$, Eq. 43 is numerically integrated regarding the droplet diameter between $d_{min}$ and $d_{max}$. Finally, the spray drift is calculated by means of Eqs. 44–46. Therefore, algebraic equations and just one integral have to be solved independently of the number of classes used to represent the atomized DSD.

**Table 4** $C_dA_n$ for ISO 10625:2018 nozzles

| Color code | $C_dA_n(10^{-6}\ m^2)$ |
|---|---|
| Orange | 0.272 |
| Green | 0.408 |
| Yellow | 0.544 |
| Light violet | 0.680 |
| Blue | 0.816 |
| Red | 1.090 |
| Brown | 1.360 |
| Grey | 1.630 |
| White | 2.180 |

It should be noted that, in a traditional Lagrangian approach, the differential equations corresponding to the mass and force balances have to be solved as a function of time for each atomized droplet size class. Therefore, the mathematical model presented in this work becomes an advantageous option over other modeling approaches for its implementation in low-resource computing systems.

## Results and discussion

### Model validation

Spray drift can be measured and reported following different protocols. To measure drift on fields, the most used protocol is the ISO 22866:2005 standard. The drift potential can be measured by conducting wind tunnel assays (ISO 22856:2008 standard) or by using a test bench (ISO 22401:2015). Although wind tunnel measurements could be used to analyze the deposition of the droplets atomized by a single nozzle, the spray drift model presented was developed to mimic the atomization from a nozzle moving with a forward velocity perpendicular to the wind direction. To validate the model, experimental results reported by Stallinga et al. (2014) were used. These authors performed spray drift trials using a single nozzle mounted on a spray carriage. The tests were carried out in an open field free of obstacles and were performed in triplicate. The spray deposits were measured using collectors located at distances from 1 to 5 m in the wind direction. The nozzle was placed 0.5 m above the ground ($H = 0.5$ m) and the forward movement speed, perpendicular to mean wind direction, was kept constant ($v_A = 2$ m/s). The nozzles used by Stallinga et al. (2014), and the calculated $\Psi$ values for each nozzle model are summarized in Table 5.

For all the trials, the deposited spray drift was reported for 9 points, distributed along the distances 0.75 and 4.75 m (the length of each interval was 0.5 m). The process variables used in the tests are shown in Table 6. From the wind speeds reported by Stallinga et al. (2014) for different heights, $U_0$ values were obtained using Eq. 25. Table 6 also includes the calculated mean wind velocity and the minimum and maximum experimental $U_0$ values.

Figure 6 shows the DSD, $d_{min}$ and $d_{crit}$ for the Lurmark 31-03-F110 nozzle, the corresponding $\Psi$ value of Table 5 and process variables of Table 6. The last two diameters allow classification of the droplets into three classes: (a) droplets that evaporate completely before reaching the objective ($d_0 < d_{min}$), (b) droplets that reach the ground surface and

**Table 5** Nozzle types used in the experimental trials (Stallinga et al., 2014)

| Trial | Nozzle | $\Psi$ $\mu m\left(\frac{m^3}{s}\right)^{-\frac{1}{3}}(Pa)^{\frac{1}{3}}(^\circ)^{\frac{2}{3}}$ |
|---|---|---|
| S1 | Lurmark 31-F110-03, Hypro, Longstanton, United Kingdom | $1.424\times10^7$ |
| S2 | XR 110–04, TeeJet, Aabybro, Denmark | $1.269\times10^7$ |
| S3 | Airmix AM OC 02, Agrotop GmbH, Obertraubling, Germany | $3.030\times10^7$ |
| S4 | Airmix AM OC 04, Agrotop GmbH, Obertraubling, Germany | $3.030\times10^7$ |
| S5 | AI UB 02, TeeJet, Aabybro, Denmark | $3.130\times10^7$ |
| S6 | AI UB 04, TeeJet, Aabybro, Denmark | $3.130\times10^7$ |
| S7 | B-Jet 02, Hardi, Nørre Alslev, Denmark | $3.169\times10^7$ |
| S8 | B-Jet 04, Hardi, Nørre Alslev, Denmark | $3.169\times10^7$ |
| S9 | IDKS 02, Lechler GmbH, Metzingen, Germany | $2.753\times10^7$ |
| S10 | IDKS 04, Lechler GmbH, Metzingen, Germany | $2.753\times10^7$ |
| S11 | IS 02, Lechler GmbH, Metzingen, Germany | $3.255\times10^7$ |
| S12 | IS 04, Lechler GmbH, Metzingen, Germany | $3.255\times10^7$ |
| S13 | AVI OC 02, Albuz, Évreux, France | $3.069\times10^7$ |
| S14 | AVI OC 04, Albuz, Évreux, France | $3.069\times10^7$ |

$\Psi$ was obtained for $P_{ref}=300$ kPa

**Table 6** Experimental process variables (Stallinga et al., 2014)

| Variable | Value |
|---|---|
| $T$(°C) | 16.1 |
| $HR$(%) | 66 |
| $U_0$ mean (m/s) | 1.71 |
| $U_0$ min (m/s) | 0.96 |
| $U_0$ max (m/s) | 2.8 |
| $H$(m) | 0.5 |
| $\Delta P$(Pa) | 300,000 |

their trajectory is modified by the wind ($d_{min} \le d_0 \le d_{crit}$) and (c) droplets that maintain their initial trajectory during flight ($d_0 > d_{crit}$). Equation 15 evaluated at $d_{min}$ gives the loss of agrochemical by volatilization (condition of total water evaporation). The difference between the result of Eq. 15 evaluated at $d_{crit}$ and at $d_{min}$, represents the droplets fraction with risk of spray drift. Since $d_{min}$ and $d_{crit}$ depend on the weather and the vertical position of the nozzle, different nozzles modify the DSD and consequently the volume fraction that each area represents.

Figure 7 compares the experimental and predicted spray drifts (126 points). Without using any fitting parameter, a good agreement between the experimental and simulated values was found for most of the tests. Trials S5 and S11, for which the predicted values show the largest deviations with respect to the experimental spray drifts, are further analyzed at the end of this section.

Figure 8a, b and c show the spray drift as a function of $x_{dep}$ for S1, S3 and S12 trials. These cases were selected because the $D_{V50}$ values are significantly different from each other (247, 459 and 621 μm, respectively). The spray drift values are presented on both

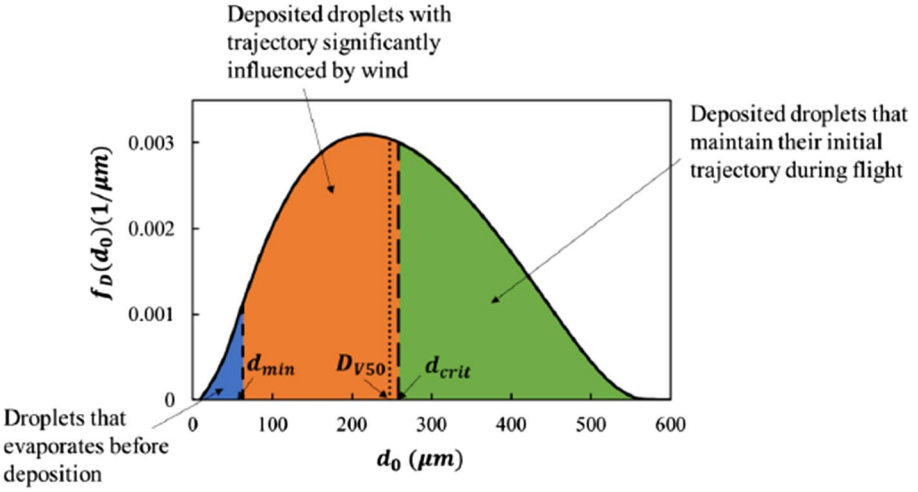


**Fig. 6** DSD and droplets classification based on characteristic diameters

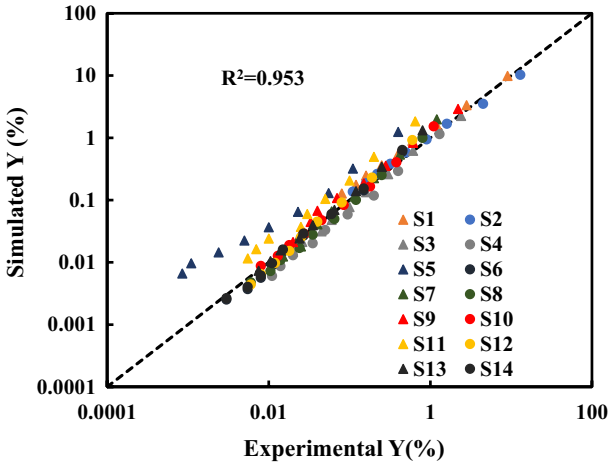


**Fig. 7** Comparison between experimental and simulated spray drift

linear (left hand side of Fig. 8) and logarithmic (right hand side of Fig. 8) scales, to favor the visualization of results in all distance ranges. As expected, for all the cases, the spray drift decreases with distance. At 1 m from the nozzle, the spray drift is approximately 9, 2 and 0.7% for the S1, S3 and S12 tests, respectively. As expected, higher spray drift values are obtained for DSDs with lower $D_{V50}$. For the S1, S3 and S12 tests, a good prediction is observed for the entire range of downwind distances, even when the spray drift is below 0.1%. Therefore, the droplets movement and size are being well represented by the model for short distances.

As previously mentioned, predictions for cases S5 and S11 show the largest deviations with respect to the experimental spray drifts. The spray drift curves corresponding to case S5 and S11 are presented in Fig. 9a and b, respectively. For these cases, the model underestimates the spray drift when the mean wind speed ($U_0$) is used. Additional simulations were

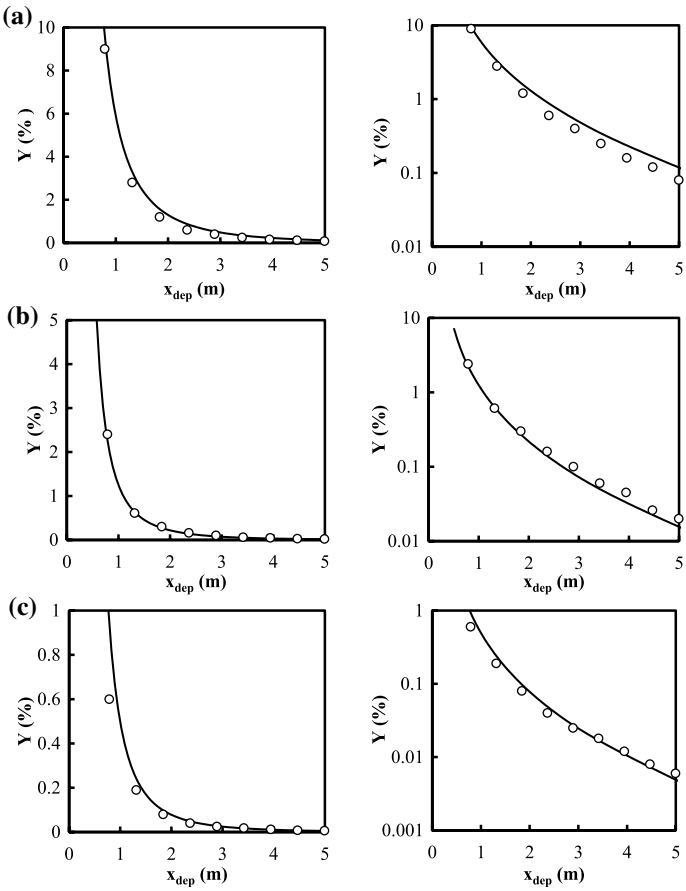


**Fig. 8** Predicted (continuous line) and experimental spray drifts (dots) as a function of downwind distance. **a** S1, **b** S3 and **c** S12

performed using the minimum and maximum speed reported by Stallinga et al. (2014). It is observed that the experimental values are between the curves obtained for the minimum and mean $U_0$. Therefore, the mathematical model predictions are satisfactory within the wind measurement uncertainties.

## Deposited DSD analysis

Considering the S1 conditions as a case study (see Tables 4, 5 and 6), Fig. 8 shows the deposited droplets diameter ($d_{dep}$) as a function of the downwind deposition distance ($x_{dep}$) for droplets whose initial angle corresponds to $\alpha = 0$ (i.e., initial vertical trajectory). Besides, Fig. 10 also presents the atomized droplet diameter ($d_0$) as a function of $x_{dep}$, calculated using Eq. 30. The higher $x_{dep}$, the higher the difference between $d_{dep}$ and $d_0$. Smaller atomized droplets are deposited at greater deposition distances. These droplets remain for longer times in flight, therefore the size reduction by evaporation is greater and makes the difference between the deposited and initial diameters more evident. According to Fig. 8, the evaporation phenomenon in droplets smaller than 100 μm is not negligible.

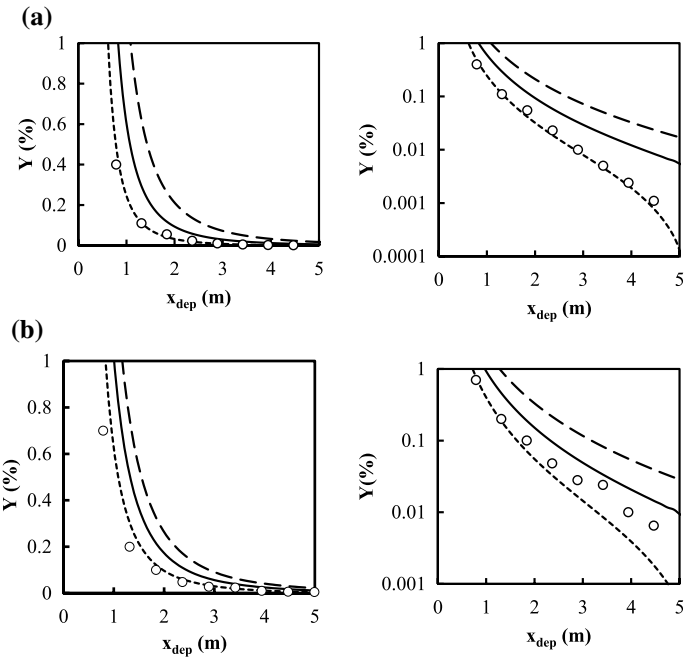


**Fig. 9** Spray drift predicted curves using mean (continuous line), minimum (short dashed line) and maximum (long dashed line) wind velocity compared to experimental values (dots) for cases **a** S5 and **b** S11

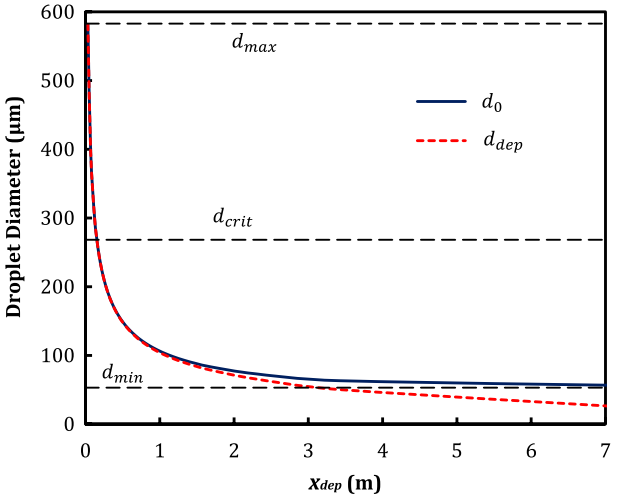


**Fig. 10** Initial ($d_0$) and deposited ($d_{dep}$) diameter of the atomized droplets with initial trajectory $\alpha = 0$ as a function of the deposition distance (case S1)

## Spray drift sensitivity analysis

The proposed model is used to analyze the spray drift changes when ±50% step changes (around the base case) of the wind speed, spray pressure and nozzle height are applied.

As an example, Fig. 11 shows the spray drifts for the base case (S1) and for those cases where positive step changes were applied.

When a + 50% change in the wind speed is imposed, a spray drift increase is observed for all deposition distances. This is caused by a greater drag force exerted on the droplets (see Eq. 33). A + 50% increase in spray pressure decreases $D_{V50}$ according to Eq. 3, leading to smaller atomized droplets. Compared to the base case, these smaller droplets are more likely to be dragged by the wind increasing the spray drift. For a + 50% change in the nozzle height, the deposition time increases. Due to the droplets remaining longer in flight, they are deposited at greater distances from the nozzle increasing spray drift. As shown in Fig. 11, spray drift is more influenced by nozzle height, followed by the wind speed and then by the spray pressure.

A 50% increase in ambient temperature produces a negligible change in spray drift (data not shown).

## Computational cost of the proposed model

To analyze the model capacity to run in a system with low computational resources, it was tested in different platforms, which are listed in Table 7. In all the tested platforms, the simulation time was less than 2 s when spray drift was evaluated at 100 distance points ($x_{dep}$). Network connection was disabled during simulations with smartphones to ensure that the calculation was performed using the smartphone processor. As the Microsoft Lumia 640 LTE was able to perform the simulations in a reasonable time, it can be concluded that the proposed model is capable of running on low computational power environments.

## Spray drift map

The software can provide traffic light labels as alerts for applicators. As an example, Fig. 12 shows a map to illustrate the results that can be numerically obtained for different scenarios using a standard 110° flat fan nozzle. The spray map was built using the simulation results

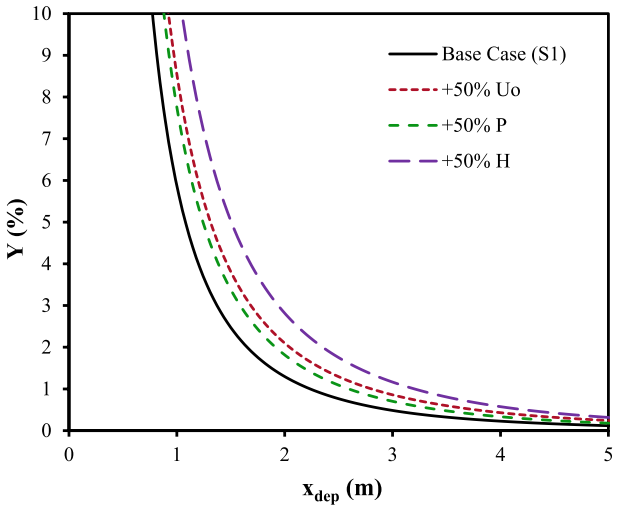


**Fig. 11** Spray drift comparison between base case S1 and atomizations with + 50% increment on wind speed, spray pressure and nozzle height

**Table 7** Platforms used to perform the simulations

| Platform | Processor | RAM (Gb) | Operative system | Implementation |
|---|---|---|---|---|
| Desktop | Intel Core i7 4790S—3.20 GHz | 8 | Microsoft Windows 7 | • Python 3.8 + Numpy 1.19 |
| Notebook | Intel Core i7 4702MQ—2.2 GHz | 8 | Microsoft Windows 10 | • Python 3.8 + Numpy 1.19<br>• Microsoft Excel |
| Motorola G6 + | ARM Cortex-A53—2.2 GHz | 4 | Android 9 | • Python 3.8 + Numpy 1.18.4<br>• Microsoft Excel |
| Samsung Galaxy J4 + | Snapdragon 425—1.4 GHz | 2 | Android 8.1 | • Microsoft Excel |
| Microsoft Lumia 640 LTE | ARM Cortex-A7—1.2 GHz | 1 | Microsoft Windows 10 Mobile | • Microsoft Excel |

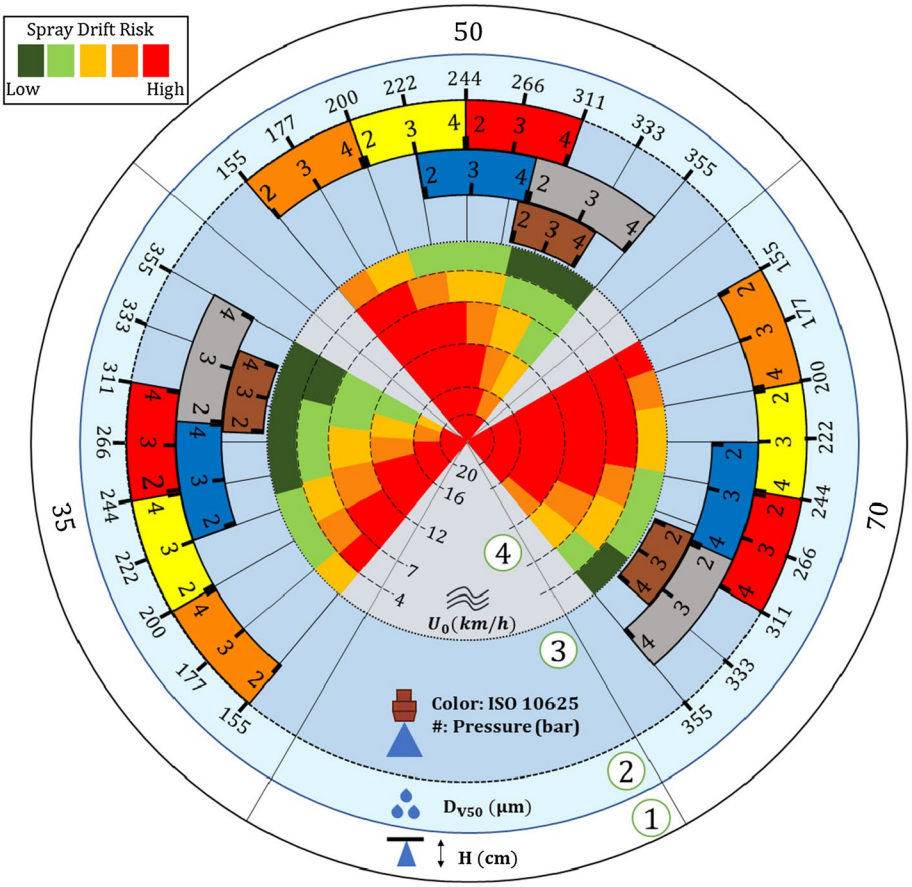


**Fig. 12** Spray drift map for a standard 110° flat fan nozzle (Color figure online)

for different wind speeds, nozzle heights and atomization pressures. Zone 3 of the map represents the input data type that the model requires for the DSD prediction (ISO classification color code and atomization pressure). This information, for each scenario, allows calculation of $D_{V50}$ diameters that are shown in Zone 2. This parameter together with the boom height ($H$) and the wind velocity ($U_0$), displayed in Zones 1 and 4 respectively, are the inputs for the spray drift model. In the inner zone of the map, the spray drift risk at $x_{dep} = 1$ m (an arbitrary distance) is presented with a colored code. For this example, spray drift values lower than 2.5% are represented by dark green, between 2.5 and 5% by light green, 5 to 7.5% by yellow, 7.5 to 10% by orange and greater than 10% by red. The software would give the spray risk as shown in Fig. 12, just selecting the nozzle, weather conditions, operating pressure and boom height.

## Conclusions

The atomized DSD from an agricultural nozzle is essential to estimate spray drift. In this work, a simple method to estimate the DSD is proposed. After analyzing atomization experimental DSD data, this distribution was successfully represented by the upper-limit log normal (ULLN) function with parameters expressed just as a function of $D_{V50}$. Also, this diameter was successfully predicted as a function of spray pressure, nozzle nominal flowrate and spray angle, which are commonly known data.

The spray drift model, based on bivariate probability density functions, was able to adequately represent experimental field data. The simulations indicate that the wind speed, nozzle height and liquid pressure have a significant influence on spray drift, while, for the studied cases, temperature and relative humidity produce negligible effects.

The spray-drift model was successfully solved in different computing platforms. The computation time was very low for all of them.

The proposed model (simple, computationally efficient and based on accessible input data) is a good basis to develop mathematical models for sprayer systems constituted by multiple nozzles aimed to be used as on-line tools. Moreover, the model can be adapted to consider other phenomena, including turbulent effects of the air and oscillations of the nozzle heights caused by the sprayer displacement.

**Acknowledgements** The authors gratefully acknowledge the financial support by the Consejo Nacional de Investigaciones Científicas y Técnicas (CONICET), the Agencia Nacional de Promoción Científica y Tecnológica (ANPCyT) and the Universidad Nacional del Sur (UNS) from Argentina.

**Data availability** Not applicable.

**Code availability** Not applicable.

## Declarations

**Conflict of interest** The authors declared that they have no conflict of interest.

## References

ASABE. (2009). *S572.1 droplet size classification*. The American Society of Agricultural and Biological Engineers.

Ashgriz, N. (2011). *Handbook of atomization and sprays*. Springer. https://doi.org/10.1007/978-1-4419-7264-4

BCPC. (1986). *Nozzle classification scheme*. British Crop Protection Council.

Bish, M. D., & Bradley, K. W. (2017). Survey of Missouri pesticide applicator practices, knowledge, and perceptions. *Weed Technology, 31*(2), 165–177.

Bodnár, T., Galdi, G. P., & Nečasová, Š. (2017). *Particles in flows*. Springer. https://doi.org/10.1007/978-3-319-60282-0

Butts, T. R., Luck, J. D., Fritz, B. K., Hoffmann, W. C., & Kruger, G. R. (2019). Evaluation of spray pattern uniformity using three unique analyses as impacted by nozzle, pressure, and pulse-width modulation duty cycle. *Pest Management Science, 75*(7), 1875–1886. https://doi.org/10.1002/ps.5352

Czaczyk, Z. (2012). Spray classification for selected flat fan nozzles. *Journal of Plant Protection Research, 52*(1), 180–183. https://doi.org/10.2478/v10045-012-0027-2

da Cunha, J. P., Reis, E. F. D., de Assunção, H. H., & Landim, T. N. (2019). Evaluation of droplet spectra of the spray tip ad 11002 using different techniques. *Engenharia Agrícola, 39*(4), 476–481. https://doi.org/10.1590/1809-4430-eng.agric.v39n4p476-481/2019

EPA – USA Environmental Protection Agency. (2001). PRN 2001-X Draft: Spray and Dust Drift Label Statements for Pesticide Products. Retrieved March 29, 2022, from https://www.epa.gov/pesticide-registration/prn-2001-x-draft-spray-and-dust-drift-label-statements-pesticide-products

Gil, E., Balsari, P., Gallart, M., Llorens, J., Marucco, P., Andersen, P. G., Fàbregasa, X., & Llopa, J. (2014). Determination of drift potential of different flat fan nozzles on a boom sprayer using a test bench. *Crop Protection, 56*, 58–68. https://doi.org/10.1016/j.cropro.2013.10.018

Guler, H., Zhu, H., Ozkan, H. E., & Ling, P. (2012). Characterization of hydraulic nozzles for droplet size and spray coverage. *Atomization and Sprays*. https://doi.org/10.1615/AtomizSpr.2012006181

Hong, S. W., Zhao, L., & Zhu, H. (2018). SAAS, a computer program for estimating pesticide spray efficiency and drift of air-assisted pesticide applications. *Computers and Electronics in Agriculture, 155*, 58–68. https://doi.org/10.1016/j.compag.2018.09.031

Hughes, R. N. (Ed.). (2013). *Behavioural mechanisms of food selection* (Vol. 20). Springer. https://doi.org/10.1007/978-3-642-75118-9

International Organization for Standardization. (2008). *ISO 22856, 2008: Equipment for crop protection-Laboratory measurement of spray drift-part 1: Wind tunnel*. International Organization for Standardization.

Kluza, P. A., Kuna-Broniowska, I., & Parafiniuk, S. (2019). Modeling and prediction of the uniformity of spray liquid coverage from flat fan spray nozzles. *Sustainability, 11*(23), 6716. https://doi.org/10.3390/su11236716

Lebeau, F., Verstraete, A., Stainier, C., & Destain, M. F. (2011). RTDrift: A real time model for estimating spray drift from ground applications. *Computers and Electronics in Agriculture, 77*(2), 161–174. https://doi.org/10.1016/j.compag.2011.04.009

Lefebvre, A. H., & McDonell, V. G. (2017). *Atomization and sprays*. Taylor & Francis, CRC Press. https://doi.org/10.1201/9781315120911

Leunda, P., Debouche, C., & Caussin, R. (1990). Predicting the transverse volume distribution under an agricultural spray boom. *Crop Protection, 9*(2), 111–114. https://doi.org/10.1016/0261-2194(90)90088-O

Løfstrøm, P., Bruus, M., Andersen, H. V., Kjær, C., Nuyttens, D., & Astrup, P. (2013). The OML-SprayDrift model for predicting pesticide drift and deposition from ground boom sprayers. *Journal of Pesticide Science*. https://doi.org/10.1584/jpestics.D12-064

Matthews, G., Bateman, R., & Miller, P. (2014). *Pesticide application methods* (4th ed.). Wiley. https://doi.org/10.1002/9781118351284

Mawer, C. J., & Miller, P. C. H. (1989). Effect of roll angle and nozzle spray pattern on the uniformity of spray volume distribution below a boom. *Crop Protection, 8*(3), 217–222. https://doi.org/10.1016/0261-2194(89)90030-6

Nuyttens, D., Baetens, K., De Schampheleire, M., & Sonck, B. (2007). Effect of nozzle type, size and pressure on spray droplet characteristics. *Biosystems Engineering, 97*(3), 333–345. https://doi.org/10.1016/j.biosystemseng.2007.03.001

Nuyttens, D., De Schampheleire, M., Verboven, P., Brusselman, E., & Dekeyser, D. (2009). Droplet size and velocity characteristics of agricultural sprays. *Transactions of the ASABE, 52*(5), 1471. https://doi.org/10.13031/2013.29127

Onorato, A., & Tesouro, M. O. (2006). *Pulverizaciones Agrícolas Terrestres* (1ra ed.) (Ground Agricultural Spraying). Instituto Nacional de Tecnología Agrícola INTA.

Post, S. L., & Hewitt, A. J. (2018). Flat-fan spray atomization model. *Transactions of the ASABE, 61*(4), 1249–1256. https://doi.org/10.13031/trans.12572

Post, S. L., Roten, R. L., & Connell, R. J. (2017). Discharge coefficients of flat-fan nozzles. *Transactions of the ASABE, 60*(2), 347–351. https://doi.org/10.13031/trans.12064

Pretty, J. (2008). (2008) Agricultural sustainability: Concepts, principles and evidence. *Philosophical Transactions of the Royal Society B: Biological Sciences, 363*(1491), 447–465. https://doi.org/10.1098/rstb.2007.2163

Pretty, J., & Bharucha, Z. P. (2014). Sustainable intensification in agricultural systems. *Annals of Botany, 114*(8), 1571–1596. https://doi.org/10.1093/aob/mcu205

Renaudo, C. A. (2020) *Modelo predictivo de la deriva de pulverización en aplicaciones agrícolas de botalón* (Spray drift model for boom sprayers). Universidad Nacional del Sur. Retrieved March 29, 2022, from http://repositoriodigital.uns.edu.ar/handle/123456789/5147

Sijs, R., Kooij, S., Holterman, H. J., Van De Zande, J., & Bonn, D. (2021). Drop size measurement techniques for sprays: Comparison of image analysis, phase Doppler particle analysis, and laser diffraction. *AIP Advances, 11*(1), 015315. https://doi.org/10.1063/5.0018667

Song, Y., Sun, H., Li, M., & Zhang, Q. (2015). Technology application of smart spray in agriculture: A review. *Intelligent Automation & Soft Computing, 21*(3), 319–333. https://doi.org/10.1080/10798587.2015.1015781

Srivastava, S., Goyal, P., & Srivastava, M. M. (2009). Pesticides: Past, present, and future. In L. M. L. Nollet & H. S. Rathore (Eds.), *Handbook of pesticides: Methods of pesticide residues analysis* (p. 628). CRC Press.

Stainier, C., Robaye, V., Destain, M. F., Schiffers, B., & Lebeau, F. (2006). Experimental evaluation of a spray drift Gaussian tilting plume model. *Aspects of Applied Biology, 77*(2), 365–370.

Stallinga, H., van de Zande, J. C., Michielsen, J. G. P., & van Velde, P. (2014). (2014) Spray drift and spray distribution of end nozzles. *International Advances in Pesticide Application, 122*, 395–400.

Stull, R. (2011). Wet-bulb temperature from relative humidity and air temperature. *Journal of Applied Meteorology and Climatology, 50*(11), 2267–2269. https://doi.org/10.1175/JAMC-D-11-0143.1

Tan, Z. (2014) Air pollution and greenhouse gases from basic concepts to engineering. In *Applications for air emission control*. Springer. https://doi.org/10.1007/978-981-287-212-8

Teske, M. E., Thistle, H. W., Riley, C. M., & Hewitt, A. J. (2016). Initial laboratory measurements of the evaporation rate of droplets inside a spray cloud. *Transactions of the ASABE, 59*(2), 487–493. https://doi.org/10.13031/trans.59.11543

Teske, M. E., Thistle, H. W., Schou, W. C., Miller, P. C. H., Strager, J. M., Richardson, B., Butler Ellis, M. C., Barry, J. W., Twardus, D. B., & Thompson, D. G. (2011). A review of computer models for pesticide deposition prediction. *Transactions of the ASABE, 54*(3), 789–801. https://doi.org/10.13031/2013.37094

Van de Zande, J. C., Holterman, H. J., & Wenneker, M. (2008) Nozzle classification for drift reduction in orchard spraying: Identification of drift reduction class threshold nozzles. *Agricultural Engineering International*. Retrieved March 27, 2022, from https://www.wur.nl/en/Publication-details.htm?publicationId=publication-way-333738363536

Van De Zande, J. C., Porskamp, H. A. J., & Holterman, H. J. (2002). Influence of reference nozzle choice on spray drift classification. *Aspects of Applied Biology, 66*, 49–56.

van den Berg, F., Kubiak, R., Benjey, W. G., Majewski, M. S., Yates, S. R., Reeves, G. L., Smelt, J. H., & van der Linden, A. M. A. (1999). Emission of pesticides into the air. *Water, Air, and Soil Pollution, 115*(1), 195–218. https://doi.org/10.1023/A:1005234329622

Villa-Henriksen, A., Edwards, G. T., Pesonen, L. A., Green, O., & Sørensen, C. A. G. (2020). Internet of Things in arable farming: Implementation, applications, challenges and potential. *Biosystems Engineering, 191*, 60–84. https://doi.org/10.1016/j.biosystemseng.2019.12.013

Wang, S. J., Dorr, G. J., Khashehchi, M., & He, X. (2015). Performance of selected agricultural spray nozzles using particle image velocimetry. *Journal of Agricultural Science and Technology, 17*(3), 601–613.

Zannetti, P. (Ed.). (2013). *Air pollution modeling: theories, computational methods and available software*. Springer. https://doi.org/10.1007/978-1-4757-4465-1